Attitude Control for a Group of Space Vehicles

António Santos

Abstract **- Attitude control is developed for a group of three space vehicles (SV). The on-board attitude apparatus is presented. Each vehicle measures the Sun vector, the Earth vector, the attitude quaternion and its angular velocity. Control actuation is provided by reaction wheels or attitude thrusters. The Wahbas attitude determination algorithm is implemented. An Extended Kalman Filter is derived for attitude estimation and additionally for gyroscope drift estimation. A control strategy for stand-alone vehicle attitude reorientation is implemented using a modified LQR design to cope with large reorientation manoeuvres. One group strategy consists in a leader following approach where inertial attitude representation is available to the entire group. A relative attitude determination algorithm is used in a scenario where two vehicles do not possess the inertial attitude instrumentation. A third strategy forces the vehicles to target a common mid-attitude point. Results for estimation, single vehicle control and group control are presented and analysed.**

I. Introduction

Although formation of vehicles in many areas has been on the spotlight for several years, formation flying of spacecraft is a relatively recent concept. A growing number of space applications have lately been identified that will utilize distributed systems of satellites. There is a great level of interest in both the scientific and defence communities to develop mature systems for autonomous rendezvous and formation flying. One of the main advantages of a multiple spacecraft approach is the reconfiguration capability, which is a synonym of multi-functionality and adaptability.

Attitude consensus is required for interferometry and many other diverse applications. Group control such that relative attitude can be maintained with high precision while mitigating disturbance effects is often a requirement. Simultaneously reconfiguration of the group attitude for multiple operation scenarios must be addressed which inevitably leads to the issue of adequate and robust reorientation manoeuvring techniques.

In this text

In section II sensors and actuators main characteristics are given. In Section III the space environment is briefly described along with orbital dynamics of Earth satellites. Section IV is dedicated estimation algorithms employed for one vehicle standalone, namely the Wahbas' problem solution, an Extended Kalman Filter (EKF) for angular velocity estimation, a Multiplicative Extended Kalman Filter for attitude and gyro drift bias estimation. Feedback control law based on LQR design for the standalone vehicle is discussed in Section V. A deterministic relative attitude method that uses line of sight measurements between three vehicles is presented in VI. Section VII is devoted to group attitude control. Scenarios where different attitude information is available are investigated. A group coordinator for monitoring and triggering operations in the group is also introduced. Simulation results are presented and analysed in Section VIII. Section IX summarizes the main conclusions and future work.

II. Sensors and actuators

The complete IMU package of the standalone SV includes one Sun sensor, one Horizon sensor or Earth sensor, one Star Tracker and one gyroscope. The actuator equipment entails a set of four reaction wheels and set of six attitude thrusters. The measurement of both the Sun sensor and Horizon sensor is the set of azimuth φ and elevation α angles of the Sun or Earth line direction in the corresponding sensor frame coordinates. The relation between angles and the direction vector is given by:

$$azim \equiv \varphi = \arctan(e_y/e_x)$$
$$elev \equiv \alpha = \arctan\left(e_z/\sqrt{e_x^2 + e_y^2}\right) \quad (1)$$

where $\boldsymbol{e}_s = \begin{bmatrix} e_x & e_y & e_z \end{bmatrix}^T$ is the true direction vector written in sensor coordinates. In order to reflect Sun sensor measurement inaccuracies Gaussian noise is added to the true angles. We define the angle set $m = [\varphi \quad \alpha]^T$. The Sun sensor measurement model is:

$$\hat{m} = m + n_{ss}$$

where $\hat{m} = [\hat{\varphi} \quad \hat{\alpha}]^T$ is the measured quantity and $n_{ss} \sim N(0, \sigma_{ss}^2 I_{2\times 2})$. A value of $\sigma_{ss} = 0{,}1°$ is established.

The Horizon sensor noise model adds an additional term:

$$n_{HS} = n_{HS,1} + n_{HS,2}$$

with $n_{HS} = \begin{bmatrix} n_\varphi & n_\alpha \end{bmatrix}^T$, $n_{HS,1} \sim N(0, \sigma_{HS,1}^2 I_3)$ with $\sigma_{HS,1} = 0{,}2°$, and $n_{HS,2} \sim N(0, \sigma_{HS,2}^2 I_3)$, where $\sigma_{HS,2} = 0{,}1\|\boldsymbol{\omega}\|$.

Star Trackers compare Star configurations with a star catalogue, providing a direct measure of attitude. The Star Tracker quaternion measurement is modelled by multiplicative quaternion error ($\delta\boldsymbol{q}$) according to:

$$\boldsymbol{q}_m = \delta\boldsymbol{q} \otimes \boldsymbol{q}_{true} \quad (2)$$

For small errors the multiplicative quaternion error can be approximately related to the following expression

$$\delta\boldsymbol{q} \approx \left[\frac{\delta\psi}{2} \; \frac{\delta\theta}{2} \frac{\delta\varphi}{2} \; 1\right]^T = \left[\frac{\boldsymbol{a}^T}{2} \quad 1\right]^T \quad (3)$$

where δφ, δψ and δθ are the three Euler angles, respectively yaw, pitch and roll. Normalizing $\delta\boldsymbol{q}_{norm} = \delta\boldsymbol{q}/\|\boldsymbol{q}\|$ it becomes an error with the formal properties of a quaternion and can be inserted directly in (2).

A rate-integrating gyroscope is used in rate mode to provide rate angular measurements. Its output is considered to be the true angular velocity of the spacecraft plus noise originated by electromechanical interference (n_v) and float torque random walk (n_u):

$$n_{RIG}(t) = n_v(t) + \int_{t_0}^{t} n_u(\tau)d\tau \quad (4)$$

Both $n_v(t)$ and $n_u(\tau)$ are modeled as Gaussian noise with zero mean, more rigorously:

$n_v \sim N(0, I_{3\times 3}\sigma_v^2)$ and $n_u \sim N(0, I_{3\times 3}\sigma_u^2)$

For a time sample of $T_s = 0{,}1\ s$ the values considered are within the typical range:

$$\sigma_v = 0{,}6957\ arcsec/s$$
$$\sigma_u = 2{,}5743 \times 10^{-4}\ arcsec/s^2$$

Reaction wheels are driven by an electric motor applying torque. The opposite torque is reflected upon the SV body. A two-phase induction motor is assumed, electronically-driven by square pulses that vary the duty cycle within the interval [-1, 1]. A linear relation between duty cycle and control voltage is typically desirable. However in reality this is not the case as the electronics face a 'dead zone' near the origin. A dead zone of $X_{dc} = 0{,}001$ is assumed.

The net torque on the wheel is given by:

$$M = X_{dc}M_{em} - M_{friction} \quad (5)$$

where M_{em} is the electromagnetic torque when the duty cycle is unity, $M_{friction}$ is the bearing friction torque dependent on the wheel speed, s. The electromagnetic torque model assumed follows the approximation given in [1].

$$M_{em} = 2M_0 \alpha r(\alpha^2 + r^2)^{-1} \quad (6)$$

where $r = 1 - s/s_{max}$ for $X_{dc} > 0$, $r = 1 + s/s_{max}$ for $X_{dc} < 0$. s_{max} is the synch speed, α is the value of r for which M_{em} has the maximum magnitude M_0. The friction torque is simply modelled as the sum of Coulomb and viscous terms:

$$M_{friction} = M_c . sgn(s) + f . s \quad (7)$$

Additionally the wheels can be modelled as perfect discs. Their characteristics are sum up in Table 1.

Table 1 – Reaction wheels nominal parameters

I^w [kg. m^2]	M_0 [N. m]	M_c [N. m]	f $[N.m.s/rad]$	s_{max} $[RPM]$	s_0 $[RPM]$
0,038	7,1628	7,06 $\times 10^{-3}$	1,21 $\times 10^{-3}$	1500	500

Thrusters produce thrust by expelling propellant in the opposite direction. Torque is generated as the thrust is decentred and applied at a certain distance from the spacecraft centre of mass as given by:

$$\boldsymbol{M} = \boldsymbol{T} \times \boldsymbol{b} \quad (8)$$

Two thruster modes will be considered: the continuous ideal thruster and the pulse thruster. In order to emulate the impulsive behaviour, the pulse thruster control input undergoes a coarse quantization for a 0,1 s pulse period. Table 2 lists the main characteristics of the thrusters for simulation.

Table 2 – Thruster parameters

b	T_{max}	M_{max}	Period	Quantization step
0,5 m	1 N	0,5 $N.m$	0,1 s	0,01 $N.m$

Usefulness of GPS signals for determining position of the satellite in ECI are proved in [7]. The measurement error is modelled as additive Gaussian noise:

$$\widehat{\boldsymbol{p}}_{GPS} = \boldsymbol{p}_{ECI} + \boldsymbol{n}_{GPS} \quad (9)$$

where $\boldsymbol{n}_{GPS} \sim N(0, \sigma_{GPS}^2)$ with $\sigma_{GPS} = 10\ m$

III. Vehicle dynamics

Keplerian orbits

Newton's laws are used to model the dynamics of translational motion of the satellite about the Earth:

$$\ddot{\boldsymbol{r}} = -\frac{\mu}{r^3}\boldsymbol{r} \quad (10)$$

with $\mu = GM$ being the gravitational constant of the Earth, $\boldsymbol{r}$ being the SV position relatively to the Earth centre in ECI coordinates, and r its norm. It is assumed that the satellite is a point mass several orders of magnitude inferior to the Earth mass, and that the Earth is a perfectly spherical object.

The initial position ($\boldsymbol{r}$) and velocity ($\boldsymbol{v}$) are the only initial parameters necessary to establish the orbit.

Viewing and lighting conditions

Two particular viewing configurations can occur during orbit: transit and occultation. Transit is the optimal situation where the SV has direct line of sight to the Sun and sees the Earth disk totally illuminated. Occultation on the other hand constitutes the worst scenario with Sunlight blockage and a dim Earth disk.

Considering the Sun as a point an approximate evaluation for the unfavourable occultation condition can be given. Let $\boldsymbol{X}$ be a vector from the Sun to the SV, $\boldsymbol{P}$ be a vector from the Sun to the centre of the Earth, and $R_\oplus$ be the radius of the Earth. Additionally consider:

$$\boldsymbol{d} = \boldsymbol{r} - \left(\frac{\boldsymbol{s_p}}{\|\boldsymbol{s_p}\|} \cdot \frac{\boldsymbol{r}}{\|\boldsymbol{r}\|}\right)\boldsymbol{r} \quad (11)$$

with $\boldsymbol{s}_p$ be the position of the Sun relatively to the Earth and $\boldsymbol{d}$ the normal component of the SV position ($\boldsymbol{r}$) to the Earth line. Occultation occurs when $R_\oplus > \|\boldsymbol{d}\|$ and $X > P$. In such case the Sun sensor does not provide data.

Model of the Sun position

Because the Earth orbit around the Sun has a relatively low eccentricity of $e = 0{,}016751$, a circular orbit is sufficient to capture its essence. The orbit radius is considered equal to the mean distance from the Earth to the Sun:

$$r_c = 1\ UA = 149597870700\ m$$

Considering the inclination of the ecliptic $i_e = 23.4°$, the position of the Sun in ECI frame is given by

$$\boldsymbol{r}_E^{ec} = r_c \begin{bmatrix} \cos\nu \\ \cos i_e \sin\nu \\ \sin i_e \sin\nu \end{bmatrix} \boldsymbol{r}_E^{ec} \quad (12)$$

where $\nu = \frac{2\pi}{T}t$ with T the orbital period.

Attitude kinematics and dynamics

Let the quaternion $\bar{q} = [\boldsymbol{q} \quad q]^T$ represent the orientation of the rigid body with respect to a reference frame. The kinematics of the quaternion is governed by the following differential equation:

$$\dot{\bar{q}} = \frac{1}{2}\Omega(\boldsymbol{\omega})\bar{q} \quad (13)$$

with $\Omega(\boldsymbol{\omega}) = \begin{bmatrix} -[\boldsymbol{\omega}\times] & \boldsymbol{\omega} \\ -\boldsymbol{\omega}^T & 0 \end{bmatrix}$.

The SV is assumed to be a rigid body in free space housing three or four reaction wheels allowed to rotate in a fixed axis with respect to the main body. Hence the total angular momentum of the entire satellite is given by:

$$\boldsymbol{H} = I\boldsymbol{\omega} + \boldsymbol{h_r} \quad (14)$$

The time derivative of $\boldsymbol{H}$ relatively to an inertial referential equals the external applied torque which can be written in the body frame coordinates as:

$$\boldsymbol{M} = \left(\frac{d\boldsymbol{H}}{dt}\right)^i = \left(\frac{d\boldsymbol{H}}{dt}\right)^b + \boldsymbol{\omega} \times \boldsymbol{H} \quad (15)$$

The term $\left(\frac{d\boldsymbol{H}}{dt}\right)^b$ is the derivative relatively to the body frame. The term $\boldsymbol{\omega} \times \boldsymbol{H}$ comprises the gyroscopic due to the SV angular rotation relatively to the inertial frame. Substitution of 14 in 15 followed by rearrangement of terms renders:

$$\left(\frac{d\boldsymbol{H}}{dt}\right)^i = I\dot{\boldsymbol{\omega}} + \boldsymbol{\omega} \times I\boldsymbol{\omega} + \left(\frac{d}{dt}\boldsymbol{h_r}\right)^b + \boldsymbol{\omega} \times \boldsymbol{h_r} \quad (16)$$

The term $\left(\frac{d}{dt}\boldsymbol{h_r}\right)^b$ is solely due to the angular acceleration of the reaction wheels:

$$\left(\frac{d}{dt}\boldsymbol{h_r}\right)^b = \frac{d}{dt}(W^I\boldsymbol{\omega}^w) = W^I\dot{\boldsymbol{\omega}}^w + \boldsymbol{\omega}^w\frac{d}{dt}W^I \quad (17)$$

Term $\boldsymbol{\omega}^w = [\omega_1^w \quad \dots \quad \omega_n^w]$ where ω_i^w is the i^{th} wheel angular velocity and $W^I = I^w W^a = I^w[\boldsymbol{e}_1 \quad \dots \quad \boldsymbol{e}_n]$ with $\boldsymbol{e}_i$ being the i^{th} wheel mounting axis, which is constant relatively to the body, hence $\frac{d}{dt}W^I = 0$. We define $\boldsymbol{M}^w$ as $\boldsymbol{M}^w = I^w\dot{\boldsymbol{\omega}}^w$ which means that M_i^w is the moment applied to i^{th} wheel accounting for electric motor torque and friction effects. This way $W^I\dot{\boldsymbol{\omega}}^w = W^a\boldsymbol{M}^w$ and (15) can be rewritten as:

$$\dot{\boldsymbol{\omega}} = I^{-1}(\boldsymbol{M} - \boldsymbol{\omega} \times I\boldsymbol{\omega} - W^a\boldsymbol{M}^w - \boldsymbol{\omega} \times W^I\boldsymbol{\omega}^w) \quad (18)$$

which is a nonlinear differential equation in $\boldsymbol{\omega}$.

The external moment $\boldsymbol{M}$ accounts for the sum of control moment by the thrusters and disturbance moments.

For simplicity we model the SV inertia as of an equivalent cylinder with radius $r_S = 0{,}4$ m, height $h_S = 1$ m and mass $m_s = 150$ kg (with the z-axis coincident with the axis of symmetry):

$$I = \begin{bmatrix} 18{,}5 & 0 & 0 \\ 0 & 18{,}5 & 0 \\ 0 & 0 & 12 \end{bmatrix} kg.m^2$$

IV. Estimation

Deterministic observer

The deterministic observer implements the solution to the Wahba's problem originally poses the question of finding matrix A that best fits the two-pair vector observations:

$$A\boldsymbol{r}_1 = \boldsymbol{b}_1$$
$$A\boldsymbol{r}_2 = \boldsymbol{b}_2$$

Determination of attitude can be achieved by the q-method solution of the Wahba's using Sun and Earth vector measurements. According to [11] Wahba introduced a loss function such that its minimization renders the proper and orthonormal matrix A for any number of pair observations greater than two

$$L(A) \equiv \frac{1}{2}\sum_i a_i |b_i - Ar_i|^2 \tag{19}$$

where $\boldsymbol{b}_i$ is a vector measured in the SV body frame and $\boldsymbol{r}_i$ the corresponding vector in the ECI reference frame. $\{a_i\}$ are non-negative weights normally assigned as the inverse of the standard deviation of the corresponding sensor, i.e. $a_i = 1/\sigma_i$.

The loss function in (19) can be rewritten as:

$$L(A) = \sum_i a_i - tr(AB^T) \tag{20}$$

with

$$B = \sum_i a_i \, \boldsymbol{b}_i \boldsymbol{r}_i^T$$

Making the quaternion attitude appear in term $tr(AB^T)$, through $A = (q_4^2 - |\boldsymbol{q}|^2)I_{3\times3} + 2\boldsymbol{q}\boldsymbol{q}^T - 2q_4[\boldsymbol{q}\times]$, and evolving it, renders:

$$tr(AB^T) = \bar{q}^T K \bar{q}$$

where K is the symmetric traceless matrix:

$$K = \begin{bmatrix} B + B^T - Itr(B) & \sum_i a_i b_i \times r_i \\ \sum_i a_i (b_i \times r_i)^T & tr(B) \end{bmatrix}$$

Hence minimization of $L(A)$ is equivalent to maximization of the modified function

$$L'(\bar{q}) = \bar{q}^T K \bar{q} \tag{21}$$

The extrema of L' subject to the normalization constrain $\bar{q}^T\bar{q} = 1$ is found by the method of Lagrange multipliers. Define the corresponding Lagrange auxiliary function.

$$G(\bar{q}) = \bar{q}^T K \bar{q} - \lambda(1 - \bar{q}^T\bar{q}) \tag{22}$$

Differentiating (20) without constrain and equalling to zero, one obtains the eigenvector equation:

$$K\bar{q} = \lambda\bar{q} \tag{23}$$

The q-method finds the optimal quaternion estimate as the normalized eigenvector with the largest eigenvalue.

$$K\bar{q}_{opt} = \lambda_{max}\bar{q}_{opt}$$

as the substitution of $K\bar{q}$ by $\lambda_{max}\bar{q}_{opt}$ in $L'(\bar{q})$ proves it. This however is unaware of the dual quaternion representation of attitude. Therefore it is most certain that discontinuities will occur via change of sign. Supervision is added to the q-method to prevent this by comparison with the previous estimate, i.e.

$$if \; \|\bar{q}_{opt_k} - \bar{q}_{opt_{k-1}}\| > \text{Threshold: do } \bar{q}_{opt_k} = -\bar{q}_{opt_k}$$

EKF for angular velocity estimation

Discretization of (18) yields:

$$\omega_{k+1} = -I^{-1}\Delta t(\boldsymbol{\omega}_k \times I\boldsymbol{\omega}_k + \boldsymbol{\omega}_k \times W^I\boldsymbol{\omega}^w) + I^{-1}\Delta t(\boldsymbol{M} - W^a\boldsymbol{M}^w) + \boldsymbol{\omega}_k \tag{24}$$

The propagation matrix $\Phi_k = \frac{\partial f}{\partial \omega_k}$ needs to be computed for the purpose of updating the covariance matrix:

$$\Phi_k = -I^{-1}\Delta t\left(\frac{\partial}{\partial\omega}(\boldsymbol{\omega}_k \times I\boldsymbol{\omega}_k) + \frac{\partial}{\partial\omega}(\boldsymbol{\omega}_k \times \boldsymbol{h}_r)\right) + \frac{\partial}{\partial\omega}\boldsymbol{\omega}_k$$

The first term in brackets decomposes into two terms:

$$\frac{\partial}{\partial\omega}(\boldsymbol{\omega}\times I\boldsymbol{\omega}) = \frac{\partial}{\partial\omega}\boldsymbol{\omega}\times I\boldsymbol{\omega} + \boldsymbol{\omega}\times\frac{\partial}{\partial\omega}(I\boldsymbol{\omega}) = I_{3\times3}\times I\boldsymbol{\omega} + \boldsymbol{\omega}\times(II_{3\times3})$$

Where the cross products between vectors and matrices are generalized as:

$$I_{3\times3}\times I\boldsymbol{\omega} = \left[\begin{bmatrix}1\\0\\0\end{bmatrix}\times I\boldsymbol{\omega} \quad \begin{bmatrix}0\\1\\0\end{bmatrix}\times I\boldsymbol{\omega} \quad \begin{bmatrix}0\\0\\1\end{bmatrix}\times I\boldsymbol{\omega}\right]$$

$$\boldsymbol{\omega}\times(II_{3\times3}) = \left[\boldsymbol{\omega}\times I\begin{bmatrix}1\\0\\0\end{bmatrix} \quad \boldsymbol{\omega}\times I\begin{bmatrix}0\\1\\0\end{bmatrix} \quad \boldsymbol{\omega}\times I\begin{bmatrix}0\\0\\1\end{bmatrix}\right]$$

Similarly the second term in brackets leads to

$$\frac{\partial}{\partial\omega}(\boldsymbol{\omega}\times\boldsymbol{h}_r) = I_{3\times3}\times\boldsymbol{h}_r = \left[\begin{bmatrix}1\\0\\0\end{bmatrix}\times\boldsymbol{h}_r \quad \begin{bmatrix}0\\1\\0\end{bmatrix}\times\boldsymbol{h}_r \quad \begin{bmatrix}0\\0\\1\end{bmatrix}\times\boldsymbol{h}_r\right]$$

The last term of Φ_k is simply $\frac{\partial}{\partial\omega}\boldsymbol{\omega}_k = I_{3\times3}$, rendering the propagation matrix in the following compact form:

$$\Phi_k = -I^{-1}dt(I_{3\times3}\times I\boldsymbol{\omega} + \boldsymbol{\omega}\times(II_{3\times3}) + I_{3\times3}\times\boldsymbol{h}_r) + I_{3\times3}$$

The observation is simply given by gyro readings affected by Additive White Gaussian Noise (AWGN):

$$\boldsymbol{z}_k = \boldsymbol{\omega}_{gyr,k} = \boldsymbol{\omega}_k + \boldsymbol{n}_{gyr,k}$$

Which is a linear observation model with sensitivity given by:

$$H_\omega = I_{3\times3}$$

The covariance of the observations assumed is:

$$R_{gyr} = E\{\boldsymbol{n}_{gyr,k}^T\boldsymbol{n}_{gyr,k}\} = \sigma_v^2 I_{3\times3}$$

MEKF for attitude and gyro drift estimation

The MEKF for quaternion estimation and gyro drift estimation uses a variant of the EKF.

For the gyro drift defined as $\boldsymbol{\mu} = \boldsymbol{\omega}_{true} - \boldsymbol{\omega}_{ref}$, the discrete model is assumed to be simply:

$$\boldsymbol{\mu}_{k+1} = \boldsymbol{\mu}_k + \boldsymbol{n}_{\omega,k} \tag{25}$$

The MEKF represents the attitude as the quaternion product (see [8] or [9]):

$$\bar{q} = \delta\bar{q}(\boldsymbol{a})\otimes\bar{q}_{ref} \tag{26}$$

Where $\delta\bar{q}$ is parameterized as in (3). The MEKF computes an estimate of the three-component vector $\boldsymbol{a}$. We remove the redundancy of the attitude representation by choosing the reference quaternion $\bar{q}_{ref}$ such that $\hat{\boldsymbol{a}}$ is identically zero, meaning that $\delta\bar{q}(\boldsymbol{0})$ is the identity quaternion.

Using the approximation $\boldsymbol{a} \approx 2\delta\boldsymbol{q}/\delta q$ it can be proven that the dynamics of $\boldsymbol{a}$ yield:

$$\dot{\boldsymbol{a}} = \left(I_{3\times3} + \frac{1}{4}diag(\boldsymbol{a}\boldsymbol{a}^T)\right)\boldsymbol{\mu} - \frac{1}{2}(\boldsymbol{\mu} + 2\boldsymbol{\omega}_{ref})\times\boldsymbol{a} \tag{27}$$

We define an auxiliary state $\boldsymbol{x}^* = [\boldsymbol{a}^T \; \boldsymbol{\mu}^T]^T$ to comply with (26). By definition $\boldsymbol{a}$ is seen as an error that parameterizes $\delta\bar{q}(\boldsymbol{a})$ rotation for each cycle. Therefore $\boldsymbol{a}$ is set to zero for the next filter iteration.

Linearization of (27) followed by discretization yields the discrete propagation equation of $\boldsymbol{a}$:

$$\boldsymbol{a}_{k+1|k} = \left(I_{3\times3} - [\boldsymbol{\omega}_{ref}\Delta t\times]\right)\boldsymbol{a}_{k|k} + \boldsymbol{n}_{a,k} \tag{28}$$

Putting together (25) and (28) in matrix form renders:

$$\boldsymbol{x}^*_{k+1|k} = \begin{bmatrix} F_k & I_{3\times3}\Delta t \\ 0 & I_{3\times3} \end{bmatrix} \boldsymbol{x}^*_{k|k} + I_{6\times6}\boldsymbol{n}_k \tag{29}$$

with $F_k = I_{3\times3} - [\boldsymbol{\omega}_{ref}\Delta t \times]$ and $\boldsymbol{n}_k = \begin{bmatrix} \boldsymbol{n}_{a,k} \\ \boldsymbol{n}_{\omega,k} \end{bmatrix}$.

The covariance error of the state $\boldsymbol{x}^*_{k+1|k}$ is propagated according to the Kalman filter rule:

$$P_{k+1|k} = \Phi_k P_{k|k} \Phi_k^T + G Q_k G^T \tag{30}$$

where $\Phi_k = \begin{bmatrix} F_k & I_{3\times3}\Delta t \\ 0 & I_{3\times3} \end{bmatrix}$ and $G = I_{6\times6}$.

The propagation of the quaternion is given by an approximate solution of (13) that assumes a constant $\boldsymbol{\omega}$ during the sampling time interval Δt:

$$\bar{q}_{k+1|k} = e^{\frac{1}{2}\Omega(\boldsymbol{\omega}_k)\Delta t}\bar{q}_{k|k} \tag{31}$$

with $\boldsymbol{\omega}_k$ taken from gyro readings and shifted $\boldsymbol{\mu}$, yielding:

$$\boldsymbol{\omega}_k = \boldsymbol{\omega}_{gyr} + \boldsymbol{\mu}_{k-1|k-1} \tag{32}$$

There are two observation models: one for the vector measurements and the other for the Star Tracker.

Sun and Earth vector measurements provide body vector measurements that are related to the corresponding vector in the inertial frame by the attitude matrix:

$$\boldsymbol{z} \equiv \boldsymbol{v}_b = h_s(\boldsymbol{a}) + \boldsymbol{n}_z = A(\bar{q})\boldsymbol{v}_i + \boldsymbol{n}_z \tag{33}$$

After applying some algebra and the same approximations for $\delta\bar{q}(\boldsymbol{a})$ as previously yields:

$$h_s(\boldsymbol{a}) = \hat{\boldsymbol{v}}_b + [\hat{\boldsymbol{v}}_b \times]\boldsymbol{a} \tag{34}$$

with $\hat{\boldsymbol{v}}_b$ being the measurement predicted by the propagated quaternion $\bar{q} = \bar{q}_{ref} = \bar{q}_{k+1|k}$:

$$\hat{\boldsymbol{v}}_b = A(\bar{q}_{ref})\boldsymbol{v}_i$$

The derivative of $h_s(\boldsymbol{a}\ )$ with respect to $\boldsymbol{x}^*$ gives the measurement sensitivity matrix:

$$H_s \equiv \frac{\partial h_s(a)}{\partial \boldsymbol{x}^*} = [[\hat{\boldsymbol{v}}_b \times] \quad 0_{3\times3}] \tag{35}$$

The Star Tracker outputs a quaternion measurement, resulting in the simple observation model:

$$\boldsymbol{z} \equiv \bar{q}_m = \bar{q} + \boldsymbol{n}_q = \delta\bar{q}(\boldsymbol{a}) \otimes \bar{q}_{ref} + \boldsymbol{n}_q \tag{36}$$

Applying the same approximations for $\delta\bar{q}(\boldsymbol{a})$ the expected measurement as holds:

$$h_T(a, \bar{q}_{ref}) = \begin{bmatrix} (I_{3\times3} - \frac{1}{2}[\boldsymbol{a} \times])\boldsymbol{q}_{ref} + \bar{q}_{4,ref}\dfrac{\boldsymbol{a}}{\boldsymbol{2}} \\ \bar{q}_{4,ref} - \dfrac{1}{2}\boldsymbol{a}^T\boldsymbol{q}_{ref} \end{bmatrix} \tag{37}$$

resulting in the following sensitivity matrix for the Star Tracker

$$H_T \equiv \frac{\partial h_T(a)}{\partial \boldsymbol{x}^*} = \begin{bmatrix} \frac{1}{2}\Xi(\bar{q}_{ref}) & 0_{4\times3} \end{bmatrix} \tag{38}$$

where $\Xi(\bar{q}) = \begin{bmatrix} q_4 I_{3\times3} + [\boldsymbol{q} \times] \\ -\boldsymbol{q}^T \end{bmatrix}$

The Kalman gain is given by:

$$K_k = P_{k+1|k} H_k \left(H_k P_{k+1|k} H_k^T + R\right)^{-1} \tag{39}$$

The covariance state can be updated using:

$$P_{k+1|k+1} = (I - K_k H_k) P_{k+1|k} \tag{40}$$

The auxiliary state $\boldsymbol{x}^*$is update is:

$$x^*_{k+1|k+1} = x^*_{k+1|k} + K_k\left(z_k - h_k\left(x^*_{k+1|k}\right)\right) \tag{41}$$

Recall that as $\boldsymbol{a}$ represents the attitude error its value before update is null, therefore. $x^*_{k+1|k} = \begin{bmatrix} \boldsymbol{a}_{k+1|k} \\ \boldsymbol{\mu}_{k+1|k} \end{bmatrix} = \begin{bmatrix} \boldsymbol{0} \\ \boldsymbol{\mu}_{k+1|k} \end{bmatrix}$.

The observation function and sensitivity matrix are given according to the type of observation:

$$\{h_k, H_k\} = \begin{cases} \{h_S, H_S\}, & \text{from Sun or Earth sensor} \\ \{h_T, H_T\}, & \text{from Star Tracker} \end{cases}$$

Lastly the error $\boldsymbol{a}_{k+1|k+1}$ updates the predicted quaternion as:

$$\bar{q}_{k+1|k+1} = \delta\bar{q}(\boldsymbol{a}_{k+1|k+1}) \otimes \bar{q}_{k+1|k}$$

Parameter Selection

The covariance of the propagation step is assumed isentropic:

$$Q_k = \begin{bmatrix} Q_{a,k} & 0 \\ 0 & Q_\mu \end{bmatrix} \tag{42}$$

While Q_μ is made constant, $Q_{a,k}$ is a function of the angular velocity of the SV:

$$Q_{a,k} = g(\|\boldsymbol{\omega}_k\| + b)^n . \left(\frac{\Delta t}{f}\right)^p I_{3\times3} \tag{43}$$

Table 3 resumes the parameter selection in (43).

Table 3 - Three-component covariance parameters

$\boldsymbol{n}$	$\boldsymbol{g}$	$\boldsymbol{b}\ [\boldsymbol{rad/s}]$	$\boldsymbol{f}\ [\boldsymbol{s}]$	$\boldsymbol{p}$
2	2,0556 $\times 10^{-8}$	3×10^{-2}	0,1	2

A constant version of Q_a is also established that equals $Q_{a,k}$ when $\boldsymbol{\omega}_k = 0$, resulting in $Q_a = \sigma_a^2 I_{3\times3}$ with $\sigma_a^2 = 1{,}85 \times 10^{-11}$.

The covariance of the Sun and Earth vector measurements is computed via the following matrix transformation

$$R_c = H_m^v R_m {H_m^v}^T$$

where R_v is the covariance of the computed vector, R_m the covariance of the angle measurements, and

$$H_m^v = \frac{\partial v}{\partial m} = \begin{bmatrix} -\sin\alpha\cos\varphi & -\cos\alpha\sin\varphi \\ -\sin\alpha\sin\varphi & \cos\alpha\cos\varphi \\ \cos\alpha & 0 \end{bmatrix}$$

For the Star Track measurement an identical covariance transformation is performed:

$$R_{ST} = H_a^q R_a \left(H_a^q\right)^T$$

where $R_a = 0{,}2388 \times 10^{-6} I_{3\times3}\ (rad/s)^2$ is the Star Tracker three-vector error covariance, and:

$$H_a^q = \frac{\partial \bar{q}}{\partial \boldsymbol{a}} = \frac{1}{2}\begin{bmatrix} (q_4 I_{3\times3} + [\boldsymbol{q} \times]) \\ -\boldsymbol{q}^T \end{bmatrix}$$

A simplified value for the Star Tracker quaternion covariance is given by extending R_a to a 4-by-4 matrix version:

$$R_{ST} = 0{,}2388 \times 10^{-6} I_{4\times4}$$

V. Control

The control strategy follows a LQR-based approach for which a linear description of the system is required. Doing so for (13) yields:

$$\Delta\dot{\bar{q}} = \frac{1}{2}\Omega(\omega_{ref})\Delta q + \frac{1}{2}\Xi(\bar{q}_{ref})\Delta\boldsymbol{\omega} \tag{44}$$

Linearization of (18) renders:

$$\begin{aligned} \dot{\boldsymbol{\omega}}_{ref} + \Delta\dot{\boldsymbol{\omega}} = I^{-1}(&\boldsymbol{M} - \boldsymbol{\omega}_{ref} \times I\boldsymbol{\omega}_{ref} - \boldsymbol{\omega}_{ref} \times I\Delta\boldsymbol{\omega} \\ &- \Delta\boldsymbol{\omega} \\ &\times I\boldsymbol{\omega}_{ref} - W^a\boldsymbol{M}^w - \boldsymbol{\omega}_{ref} \times W^I\boldsymbol{\omega}_w - \Delta\boldsymbol{\omega} \times W^I\boldsymbol{\omega}_w) \end{aligned} \tag{45}$$

Where $\boldsymbol{\omega}_{ref}$ is the reference angular velocity distancing $\Delta\boldsymbol{\omega}$ from the true angular velocity. Additionally define trim components of the control inputs, $\boldsymbol{M}_{trim}$ and $(\boldsymbol{M}^w)_{trim}$:

$$\boldsymbol{M} = \boldsymbol{M}_{trim} + \Delta\boldsymbol{M} \qquad \boldsymbol{M}^w = (\boldsymbol{M}^w)_{trim} + \Delta\boldsymbol{M}^w \tag{46}$$

The trimming inputs have the purpose of counteracting gyroscopic effects by forcing $\dot{\boldsymbol{\omega}}_{ref} = 0$, whilst $\Delta\boldsymbol{M}$ and $\Delta\boldsymbol{M}^w$ are the deviation controls. The two components are computed separately. The thrusters trim control yields:

$$\boldsymbol{M}_{trim} = \boldsymbol{\omega}_{ref} \times I\boldsymbol{\omega}_{ref} + \boldsymbol{\omega}_{ref} \times W^I\boldsymbol{\omega}_w \tag{47}$$

The reaction wheels trim controls yields:

$$W^a(\boldsymbol{M}^w)_{trim} = -\boldsymbol{\omega}_{ref} \times I\boldsymbol{\omega}_{ref} - \boldsymbol{\omega}_{ref} \times W^I\boldsymbol{\omega}_w \tag{48}$$

The deviation control component is intended to extinguish the deviations from the references. The dynamics of the deviation terms are given by:

$$\begin{aligned} \Delta\dot{\boldsymbol{\omega}} = I^{-1}\big(&\Delta\boldsymbol{M} - \boldsymbol{\omega}_{ref} \times I\Delta\boldsymbol{\omega} - \Delta\boldsymbol{\omega} \times I\boldsymbol{\omega}_{ref} - \Delta\boldsymbol{\omega} \\ &\times W^I\boldsymbol{\omega}_w - W^a\Delta\boldsymbol{M}^w\big) \end{aligned} \tag{49}$$

Terms in $\Delta\boldsymbol{\omega}$ can be grouped by inverting the sign and order of the cross products ($a \times b = -b \times a$) yielding:

$$\Delta\dot{\boldsymbol{\omega}} = I^{-1}\big(\Delta\boldsymbol{M} + \big(-[\boldsymbol{\omega}_{ref}\times]I + [I\boldsymbol{\omega}_{ref}\times] + [W^I\boldsymbol{\omega}_w\times]\big)\Delta\boldsymbol{\omega} - W^a\Delta\boldsymbol{M}^w\big) \quad (50)$$

The LQR is devoted to linear systems described by general linear differential equations of the form $\dot{\boldsymbol{x}} = A\boldsymbol{x} + B\boldsymbol{u}$.

$$\dot{\boldsymbol{x}} = A\boldsymbol{x} + B\boldsymbol{u} \quad (51)$$

The goal of the LQR is to regulate $\boldsymbol{x}$ to zero. In addition recall that the linearization in the previous analysis provided a vector state which is the stack of the deviation vectors from the references.

$$\boldsymbol{x} = \begin{bmatrix} \Delta q \\ \boldsymbol{\Delta\omega} \end{bmatrix} \quad (52)$$

Hence the LQR control component computes the needed actuation to null the deviations to the reference augmented vector $x_{ref} = \begin{bmatrix} \bar{q}_{ref} \\ \boldsymbol{\omega}_{ref} \end{bmatrix}$.

The cost function of the LQR is defined as the following integral over time:

$$J = \int_0^\infty \big(x(t)^T Q x(t) + u(t)^T R u(t)\big)dt \quad (53)$$

Minimization of J leads to a feedback given by:

$$u(t) = -Kx(t)$$

where $K = R^{-1}B^T P$ with P resulting from the solution of the Riccati algebraic equation:

$$PA + A^T P - PBR^{-1}B^T P + Q = 0$$

Grouping equations (44) and (50) the desired state space representation is obtained with:

$$A = \begin{bmatrix} -\frac{1}{2}[\boldsymbol{\omega}_{ref}\times] & \frac{1}{2}(q_{ref,4}\, I_{3\times3} - [\boldsymbol{q}_{ref}\times]) \\ 0_{3\times3} & I^{-1}\big(-[\boldsymbol{\omega}_{ref}\times]I + [I\boldsymbol{\omega}_{ref}\times] + [W^I\boldsymbol{\omega}_w\times]\big) \end{bmatrix}$$

And

$$B = \begin{bmatrix} 0_{3\times3} \\ B' \end{bmatrix}$$

Where $\{B', \boldsymbol{u}\} = \begin{cases} \{I^{-1}, \Delta\boldsymbol{M}\} & \text{with thrusters} \\ \{-I^{-1}W^a, \Delta\boldsymbol{M}^w\} & \text{with reaction wheels} \end{cases}$

Manoeuvre Supervisor and the MLQR

The function of the manoeuvre supervisor is to establish the reference values ($\bar{q}_{ref}$, $\boldsymbol{\omega}_{ref}$, $(\boldsymbol{\omega}_w)_{ref}$) used in the linearization computed by the Modified LQR (MLQR). The supervisor collects the relevant data that influence the dynamics, namely $\bar{q}_{est}$, $\boldsymbol{\omega}_{est}$, $(\boldsymbol{\omega}_w)_{ref}$ as well as the target attitude $\bar{q}_{target}$, it monitors these values and compares them with the current reference. When the differences become larger than a given threshold it triggers a flag indicating the MLQR block that it must update its gains by linearizing around new points of reference. The algorithm of the supervisor is resumed below for the case of $\bar{q}_{target}$.

$sets\_ref(\bar{q}_{target}, \bar{q}_{est}, \boldsymbol{\omega}_{est}, \boldsymbol{\omega}_w)$	$\bar{q}^p_{ref}, \boldsymbol{\omega}^p_{ref}, \boldsymbol{\omega}^p_w$ the previous reference values
$\bar{q}_{rot} = \bar{q}_{est} \otimes q^{-1}_{target}$ $\delta\theta_1 = 2\text{acos}(\bar{q}_{rot,4})$	
$if\ \delta\theta_1 \le threshold_1$: $\quad \bar{q}_{ref} = \bar{q}_{target};\ \bar{q}^p_{ref} = \bar{q}_{target}$	
$else$: $\quad \bar{q}_{rot_2} = \bar{q}_{est} \otimes (\bar{q}^p_{ref})^{-1}$ $\quad \delta\theta_2 = 2\text{acos}(\bar{q}_{rot_2,4})$ $\quad if\ \delta\theta_2 \le threshold_2$: $\quad\quad \bar{q}_{ref} = \overline{\delta q}_{rot} \otimes \bar{q}_{est};$	$\overline{\delta q}_{rot}$ is a 10° rotation in the direction of $\bar{q}_{target}$
$\quad else: \bar{q}_{ref} = \bar{q}^p_{ref}$	
$if\ \|\boldsymbol{\omega}_{ref,1} - \boldsymbol{\omega}_{est}\| > threshold_{\omega 1}$: $\quad \boldsymbol{\omega}_{ref,1} = \boldsymbol{\omega}_{est}$	
$else: \boldsymbol{\omega}_{ref,1} = \boldsymbol{\omega}^p_{ref}$	
$if\ \|\boldsymbol{\omega}_w - \boldsymbol{\omega}^p_w\| > threshold_w$: $\quad (\boldsymbol{\omega}_w)_{ref} = \boldsymbol{\omega}_w$	
$else: (\boldsymbol{\omega}_w)_{ref} = \boldsymbol{\omega}^p_w$	
$if\ \|\boldsymbol{\omega}_{ref,1} - \boldsymbol{\omega}_{est}\| > threshold_{\omega 1}$: $\quad \boldsymbol{\omega}_{ref,1} = \boldsymbol{\omega}_{est}$	
$if\ \delta\theta_1 < threshold_3: \boldsymbol{\omega}_{ref,2} = 0$	
$else: \boldsymbol{\omega}_{ref,2} = \frac{\boldsymbol{q}_{rot}}{\sin\left(\frac{\delta\theta_1}{2}\right)} \frac{\delta\theta_1}{pi}$	
$Update\_ref()$	Update internal references

The MLQR is responsible to update the gain whenever any of the reference variables $\bar{q}_{est}$, $\boldsymbol{\omega}_{ref,1}$ or $(\boldsymbol{\omega}_w)_{ref}$ used in the linearization is updated by the supervisor. For control with thrusters it renders:

$$\boldsymbol{M}_{trim} = \boldsymbol{\omega}_{ref,1} \times \big(I\boldsymbol{\omega}_{ref,1} + W^I(\boldsymbol{\omega}_w)_{ref}\big) \quad (54)$$

In the same way, for control with reaction wheels:

$$\boldsymbol{M^w}_{trim} = -W^{a+}\Big(\boldsymbol{\omega}_{ref,1} \times \big(I\boldsymbol{\omega}_{ref,1} + W^I(\boldsymbol{\omega}_w)_{ref}\big)\Big) \quad (55)$$

where W^{a+} is defined as the pseudo inverse of $W^{\boldsymbol{a}}$.

The proposed MLQR and manoeuvre supervisor are tied in the loop rendering the modified control mechanism depicted in the block diagram of Figure 1. The supervisor informs the controller when it should update the LQR gains. The controller computes the actuators controls for incremental regulation control as well as the trimming components.

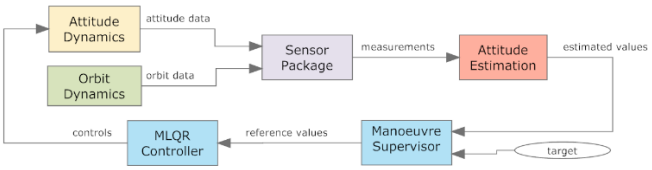

Figure 1 - Block Diagram for control with supervised MLQR

Adaptation for relative attitude tracking

When only relative information is available, the control quest becomes the nulling of relative attitude. Hence the supervisor must be adapted to cope with inputs of the form $\bar{q}_{21}$ (the attitude of frame 2 relatively to frame 1) for instance, instead of the pair target and estimate quaternions. The simple setting of $\bar{q}_{rot} = \bar{q}_{21}$ in the previous algorithm renders the solution. In fact this is equivalent to shifting the target to $\bar{q}_{target} = [0 \quad 0 \quad 0 \quad 1]^T$, i.e. a null rotation, and regarding the estimate as $\bar{q}_{est} = \bar{q}_{21}$. No additional changes are needed.

Wheel reset operation

During a wheel reset operation information about the applied wheel torques is necessary for compensation by the thrusters trimming control component:

$$\boldsymbol{M}_{trim} = \boldsymbol{\omega}_{ref} \times \big(I\boldsymbol{\omega}_{ref} + W^I\boldsymbol{\omega}_w\big) + W^a\boldsymbol{M^w}$$

Each wheel speed is reset to zero through the commanded torque computed in the following manner:

$$M^{\boldsymbol{c}} = -K_w\omega_w$$

Recalling that the dynamics of the wheel is a simple integrator: $\dot{\omega}_w = M^c/I^w$, it renders the following equation for the commanded wheel:

$$\dot{\omega}_w = -\frac{K_w}{I^w}\omega_w$$

The above differential equation constitutes a first order linear system with pole at $s_1 = -\frac{K_w}{I^w}$. The value of K_w defines the pole which is chosen to be at $\lambda = -\frac{1}{40}\ rad/s$.

VI. Relative Attitude

Relative Attitude Determination

The technique presented here for relative attitude determination employs the use of Line of Sight (LOS) vectors obtained through projection of beacon beams in a Focal Plane Detector (FPD). Each SV possesses a source (beacon) and a FPD. The beacon targets the FPD of the other SV while simultaneously its own FPD is illuminated. The FPD translates the relative position between two SV in the frame of the vehicle where it is installed.

A deterministic solution is available for a minimum of three vehicles. If a formation is constituted by four or more SV, then all combinations of three SV can be used to provide relative attitude determination.

In Figure 2 the three SV group is illustrated along with the aforementioned LOS vectors. One of the SVs is considered the group chief whereas the other are called deputies.

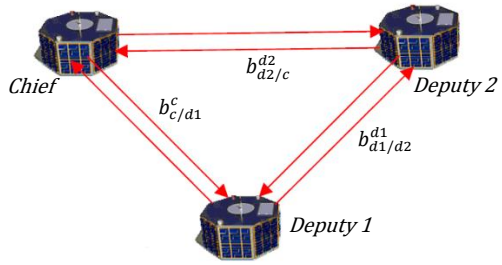

Figure 2 - Three vehicle configuration and respective LOS

The notation here follows the following rule: a subscript will describe the vehicle for which the LOS is taken both from and to, while a superscript will denote in which reference frame the LOS is both represented and measured. For example, $\boldsymbol{b}^{x}_{x/y} = -\boldsymbol{b}^{x}_{y/x}$. The frame work for relative attitude herein is not the quaternion as done in previous sections, but the attitude matrix with notation A^{y}_{x} instead, mapping coordinates expressed in the χ-frame into coordinates in the y-frame.

The beams between vehicles are assumed to be parallel, so that common vectors are given between SVs but in different coordinates. In order to accomplish this in practice a feedback mechanism must exist that monitors and corrects any misalignments. The formulation presented next follows [15].

The Sensor Model

The direct measures for all LOS observations are the image space projections (α, β). Denoting the measurement image vector $\boldsymbol{m} = [\alpha, \beta]^T$. The measurement model follows

$$\widetilde{\boldsymbol{m}} = \boldsymbol{m} + \boldsymbol{n}_m \tag{56}$$

A typical noise model used to describe the uncertainty in the focal plane coordinate observations is given as

$$R_{FOCAL} = \frac{\sigma_m^2}{1 + d(\alpha^2 + \beta^2)} \begin{bmatrix} (1 + d\alpha^2)^2 & (d\alpha\beta)^2 \\ (d\alpha\beta)^2 & (1 + d\alpha^2)^2 \end{bmatrix} \tag{57}$$

Where σ_m^2 is the variance of the measurement errors associated with α and β and d is coefficient of an order of magnitude of 1.

The focal plane observations must be converted to unit space LOS observations assuming a focal length of unity:

$$\boldsymbol{b} = \frac{1}{\sqrt{1 + \alpha^2 + \beta^2}} \begin{bmatrix} \alpha \\ \beta \\ 1 \end{bmatrix} \tag{58}$$

The unity measurement vector becomes

$$\widetilde{\boldsymbol{b}} = \boldsymbol{b} + \boldsymbol{n}_b \tag{59}$$

where $\boldsymbol{n}_b \sim N(0, \Omega)$ assuming that a normally distributed image-space vector renders an approximately Gaussian distribution over the unit space LOS vector.

Although the LOS measurement is a unit vector, it must lie on a sphere, leading to a rank deficient matrix in $\mathcal{R}^3$.

The formulation presented here follows a first-order Taylor series approximation about the focal-plane axes. The partial derivative operator $H = \frac{\partial \boldsymbol{b}}{\partial \boldsymbol{m}}$ is used to linearly expand the focal-plane covariance in (57), yielding:

$$H = \frac{1}{\sqrt{1 + \alpha^2 + \beta^2}} \begin{bmatrix} 1 & 0 \\ 0 & 1 \\ 0 & 0 \end{bmatrix} - \frac{1}{\sqrt{1 + \alpha^2 + \beta^2}} \boldsymbol{b}\boldsymbol{m}^T \tag{60}$$

Applying this operator to the uncertainty in the image space LOS vector gives the WFOV covariance model:

$$\Omega = H\, R^{FOCAL} H^T \tag{61}$$

Determination algorithm

The LOS equations for each vehicle pair are given by

$$\boldsymbol{b}^{c}_{c/d1} = A^{c}_{d1} \boldsymbol{b}^{d1}_{c/d1} \tag{62}$$

$$\boldsymbol{b}^{c}_{c/d2} = A^{c}_{d2} \boldsymbol{b}^{d2}_{c/d2} \tag{63}$$

$$\boldsymbol{b}^{d2}_{d2/d1} = A^{d2}_{c} A^{c}_{d1} \boldsymbol{b}^{d1}_{d2/d1} = A^{d2}_{d1} \boldsymbol{b}^{d1}_{d2/d1} \tag{64}$$

The LOS vectors considered in Eqs. (62)-(64) are the true LOS vectors. These are substituted by their corresponding measured LOS vectors in real operation.

Performing the inner product between both members of (62) and (63) yields:

$$\boldsymbol{b}^{c^T}_{c/d2} \boldsymbol{b}^{c}_{c/d1} = \boldsymbol{b}^{d2^T}_{c/d2} A^{d2}_{d1} \boldsymbol{b}^{d1}_{c/d1} \tag{65}$$

Equations (63) and (64) represent a direction and an arc-length respectively. The algorithm to determine A^{d2}_{d1} is given in [18] and it is briefly reviewed here.

In more general terms, the direction cosine matrix (DCM) A satisfies the following relations:

$$\boldsymbol{w}_1 = A\boldsymbol{v}_1 \tag{66}$$

$$d = \boldsymbol{s}^T A \boldsymbol{v}_2 \tag{67}$$

with the arc-length d and all vectors in Eqs. (66) and (67) being given. All vectors have unit length. The solution is given by

$$A = R(\widehat{\boldsymbol{w}}_1, \theta) A_0 \tag{68}$$

where A_0 is any DCM satisfying $\boldsymbol{w}_1 = A_0 \boldsymbol{v}_1$, and $R(\widehat{\boldsymbol{w}}_1, \theta)$ is matrix representing rotation about the $\boldsymbol{w}_1$ axis through an angle θ $(0 \le \theta < 2\pi)$ which must be also determined. By Euler's formula a rotation $R(\boldsymbol{n}, \theta)$ is given by:

$$R(\widehat{\boldsymbol{w}}_1, \theta) = \cos(\theta)\, I_{3\times 3} + (1 - \cos\theta)\boldsymbol{n}\boldsymbol{n}^T + \sin\theta\, [\boldsymbol{n}\times] \tag{69}$$

The strategy is such that first we find a candidate matrix A_o which satisfies $\boldsymbol{w}_1 = A\boldsymbol{v}_1$ and then determine the values of θ for which Eq. (67) is also satisfied. Let us look for A_o of the form

$$A_0 = R(\boldsymbol{n}_0, \theta_0) \tag{70}$$

For the special case $\boldsymbol{w}_1 = \boldsymbol{v}_1$, the choice of $\boldsymbol{n}_0$ is arbitrary provided we choose $\theta_0 = 0$. Likewise, for the case that $\boldsymbol{w}_1 = -\boldsymbol{v}_1$ choose n_0 to be any direction perpendicular to $\boldsymbol{v}_1$ and $\theta_0 = \pi$. In all other cases one might choose

$$\boldsymbol{n}_0 = \frac{\boldsymbol{w}_1 \times \boldsymbol{v}_1}{|\boldsymbol{w}_1 \times \boldsymbol{v}_1|} \tag{71}$$

When $\boldsymbol{w}_1 \neq \pm \boldsymbol{v}_1$, i.e. $\boldsymbol{w}_1$ and $\boldsymbol{v}_1$ are linearly independent, a unique solution exists for θ_0

$$\theta_0 = \arctan_2(|\boldsymbol{w}_1 \times \boldsymbol{v}_1|, (\boldsymbol{w}_1 . \boldsymbol{v}_1)) \tag{72}$$

Yielding matrix A_0 the following formula:

$$A_0 = I_{3\times 3} + [(\boldsymbol{w}_1 \times \boldsymbol{v}_1)\times] + \frac{1}{1 + \boldsymbol{w}_1 . \boldsymbol{v}_1} [(\boldsymbol{w}_1 \times \boldsymbol{v}_1)\times]^2 \tag{73}$$

Now to compute θ define

$$\boldsymbol{w}_3 = A_0 \boldsymbol{v}_2 \tag{74}$$

Then θ must obey the following equation equivalent to Eq. (67)

$$\boldsymbol{s}^T R(\boldsymbol{w}_1, \theta)\boldsymbol{w}_3 = d_2 \quad (75)$$

Substituting Euler's formula and rearranging terms leads to

$$B\cos(\theta - \beta) = (\boldsymbol{s}.\boldsymbol{w}_1)(\boldsymbol{w}_1.\boldsymbol{w}_3) - d_2 \quad (76)$$

with

$$B = |\boldsymbol{s} \times \boldsymbol{w}_1||\boldsymbol{w}_1 \times \boldsymbol{w}_3| \quad (77)$$

$$\beta = arctan_2\left(\boldsymbol{s}(\boldsymbol{w}_1 \times \boldsymbol{w}_3), \boldsymbol{s}.\left(\boldsymbol{w}_1 \times (\boldsymbol{w}_1 \times \boldsymbol{w}_3)\right)\right) \quad (78)$$

For a solution in θ, Eq. (76) poses the following necessary condition

$$|(\boldsymbol{s}.\boldsymbol{w}_1)(\boldsymbol{w}_1.\boldsymbol{w}_3) - d_2| \leq |\boldsymbol{s} \times \boldsymbol{w}_1||\boldsymbol{w}_1 \times \boldsymbol{w}_3| \quad (79)$$

If this condition holds, then

$$\theta = \beta + \arccos\left[\frac{(\boldsymbol{s}.\boldsymbol{w}_1)(\boldsymbol{w}_1.\boldsymbol{w}_3) - d_2}{|\boldsymbol{s} \times \boldsymbol{w}_1||\boldsymbol{w}_1 \times \boldsymbol{w}_3|}\right] \quad (80)$$

Because the $arccos$ function is two valued over the interval $[0, 2\pi[$ we choose the solution which better fits the given LOS data. This means we shall choose θ such:

$$\theta = \arg\min_{\theta}\{|d - s^T A v_2|\} \quad (81)$$

If one set of vectors cannot satisfy inequality (79) then another set from the formation must be used, which will naturally determine a different relative attitude. For the sake of abbreviation the algorithm just presented is named First Attitude Matrix Determination (FAMD).

When the first attitude matrix is determined the second matrix can be determined using the well-known TRIAD algorithm (see [18] for complete derivation):

$$A = M_c M_d^T \quad (82)$$

$$M_c = \left[c_1 \quad \frac{c_1 \times c_2}{\|c_1 \times c_2\|} \quad \frac{c_1 \times (c_1 \times c_2)}{\|c_1 \times (c_1 \times c_2)\|}\right] \quad (83)$$

$$M_d = \left[d_1 \quad \frac{d_1 \times d_2}{\|d_1 \times d_2\|} \quad \frac{d_1 \times (d_1 \times d_2)}{\|d_1 \times (d_1 \times d_2)\|}\right] \quad (84)$$

For instance knowledge of A_{d1}^{d2}, renders A_c^{d1} selecting $\boldsymbol{c}_1 = \boldsymbol{b}_{c/d1}^{c}$, $\boldsymbol{c}_2 = \boldsymbol{b}_{c/d2}^{c}$, $\boldsymbol{d}_1 = \boldsymbol{b}_{c/d1}^{d1}$ and $\boldsymbol{d}_2 = A_{d1}^{d2^T}\boldsymbol{b}_{c/d2}^{d2} = \boldsymbol{b}_{c/d2}^{d1}$.

Failure in finding the first attitude matrix would imply failure of the whole strategy. In order to circumvent this, logic is introduced to allow various attempts of determining the attitude matrix firstly computed in the FAMD.

VII. Group

Adequate group control is achieved by assigning the appropriate attitude target for each individual vehicle. If two SV do not possess the full IMU package, communication of one absolute estimate between SVs allows an estimate of the other SV absolute attitude; for instance for SV2 and SV3 we get:

$$\bar{q}_2 = \bar{q}_{21} \otimes \bar{q}_1$$
$$\bar{q}_3 = \bar{q}_{31} \otimes \bar{q}_1$$

where $\bar{q}_1$ is computed by SV1 using the full sensor package and $\bar{q}_{21}$, $\bar{q}_{31}$ are given by the LOS relative attitude algorithm. This information can be used directly in two ways:

1) the deputies track the chief while it manoeuvres to an assigned target.

2) the chief reorients to the target while the deputies remain stationary. As soon as the chief SV stabilizes around the target, the deputies are allowed to align their attitude with the chief.

A Group Coordinator (GC) is implemented to address the aforementioned behaviours and additional to monitor and to take decisions including:

1. establishing the different attitude targets for each SV
2. receiving information from the local SV supervisor and providing feedback
3. commanding generalized operations such as nulling of reaction wheels speed or forcing change of the estimation algorithm.

The GC allows another type of group manoeuvre that does not necessarily drive the constellation to a specified target. In this manoeuvre each SV tracks a varying target attitude, from now on called the converse attitude. For instance for SV1 its converse attitude is the attitude point between the attitudes of SV2 and SV3, i.e.

$$\bar{q}_{con_1} = f(\bar{q}_2, \bar{q}_3)$$

where f performs the following operations:

$$\bar{q}_{32} = \bar{q}_3 \otimes \bar{q}_2^{-1}$$
$$\theta_{half_{32}} = arccos(q_{32})$$
$$\boldsymbol{e}_{32} = \boldsymbol{q}_{32}/\sin(\theta_{32})$$
$$\bar{q}_{half_{32}} = \left[\boldsymbol{e}_{32}\sin\left(\frac{\theta_{32}}{2}\right) \quad cos\left(\frac{\theta_{32}}{2}\right)\right]$$
$$\bar{q}_{con_1} = \bar{q}_{half_{32}} \otimes \bar{q}_2$$

Hence the SVs approach each other towards a common point that can be seen conceptually as the centre of attitude of the initial group configuration.

When the attitude differences between the SVs become smaller than a certain threshold angle, an average common attitude is imposed to the group according to:

$$\boldsymbol{Q}_w = \frac{\bar{q}_1 + \bar{q}_2 + \bar{q}_3}{3}$$

which is normalized to $\bar{q}_w = \boldsymbol{Q}_w/\|\boldsymbol{Q}_w\|$. The threshold is set to 1° of angular separation between any combinations of two vehicles.

VIII. Results

The parameters for simulation are given here.

Table 3 summarizes the sensor accuracies set for the simulation.

Table 3 - Sensor RMS noise

σ_{ST}	0,0485°
σ_{SS}	0,1°
$\sigma_{HS,1}$	0,2°
$\sigma_{HS,2}$	$0{,}5°/s$
σ_v	$0{,}6957\ arcsec/s$
σ_u	$2{,}5743 \times 10^{-4}\ arcsec/s^2$

In this section position values are given in m, velocity values given in m/s, angles in degree and angular velocities in $°/s$ unless explicitly expressed otherwise.

Deterministic Attitude Observer

The estimation results using the deterministic observer can be seen in Figure 3. The initial conditions are: true quaternion set to $\bar{q} = [0{,}3948 \quad 0{,}5090 \quad -0{,}4679 \quad 0{,}6051]^T$, SV at rest ($\boldsymbol{\omega} = 0$), initial orbital condition in ECI coordinates with $r_{init} = [0 \quad 9400000 \quad 0]^T$ and $v = [6400 \quad 0 \quad 0]$. Furthermore we assume date is the 21st of March which simplifies the initial Sun position in ECI frame, $p_{Sun} = 1UA \times [1 \quad 0 \quad 0]^T$. This last assumption will remain for the following simulations. The corresponding estimation RMS error is $\sigma_{obs} = 0{,}2025°$.

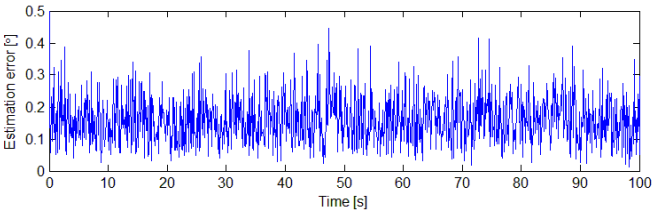

Figure 3 - Deterministic Observer error

Kalman Filter for angular velocity

The EKF for angular velocity is tested with the following filter parameters:

$Q_\omega = 10^{-14} I_{3\times3}$

$R_{gyr} = \sigma_v^2 I_{3\times3}$ with $\sigma_v = 0{,}6957\ arcsec/s$

The initial conditions set for the simulation are $\boldsymbol{\omega}_{init} = [-0{,}0336 \quad -0{,}0044 \quad -0{,}0085]\ rad/s$ implying ($\|\boldsymbol{\omega}_{init}\| = 2°/s$), a relatively high angular velocity for reorientation manoeuvres. A comparison between the filter estimate and the gyroscope error is depicted in Figure 4.

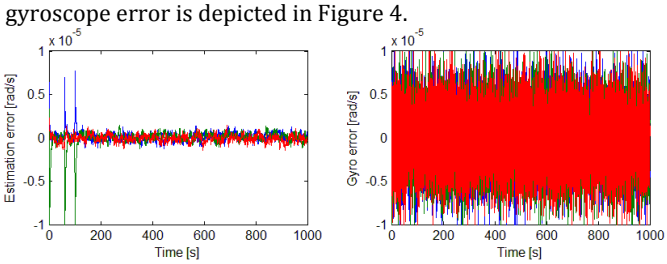

Figure 4 - Comparison between EKF and gyroscope error

MEKF for Attitude Estimation

The MEKF with constant parameters is tuned with the following values:

$$Q_a = \sigma_a^2 I_{3\times3} = 1{,}85 \times 10^{-11} I_{3\times3}$$
$$Q_\mu = \sigma_\mu^2 I_{3\times3} = 10^{-16} I_{3\times3}$$
$$R_{Sun} = 3{,}5 \times 10^{-6}$$
$$R_{Earth} = 3{,}5 \times 10^{-6}$$

The results of a MEKF exclusively for attitude estimation are presented in Figure 5. The observations are the Sun and Earth vector measurements.

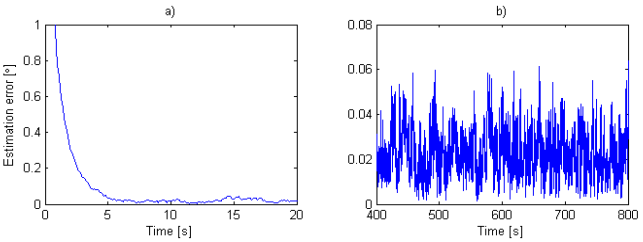

Figure 5 – Estimation with MEKF for attitude exclusively: a) convergence b) steady-state

The simulation conditions are:

$\bar{q}_{\text{true}} = [0{,}3948 \quad 0{,}5090 \quad -0{,}4679 \quad 0{,}6051]^T$, the initial estimate is $\bar{q}_{\text{init}} = [0 \quad 0 \quad 0 \quad 1]^T$. The angular velocity is $\boldsymbol{\omega} = 0$, corresponding to an initial angular error of $\theta_{err}^{init} = 72.4°$.

As observed error reaches the 0,1° line in less than 5 s. The steady-state RMS error is $\sigma_{est} = 0{,}0274°$. If a better initial guess with $\theta_{err}^{init} = 0.2°$ is chosen along with lower initial covariance $\sigma_a^2 = 10^{-6}$, the RMS error decreases to $\sigma_{est} = 0{,}0094°$ which constitutes an accuracy 21,32 times better than the one with the deterministic observer.

The MEKF estimation results using Star Tracker data are depicted in Figure 6. The corresponding RMS error is $\sigma_{est} = 0{,}0024° = 8{,}7325\ arcsec$. This means a gain in accuracy of approximately 20 times relatively to Star Tracker observations.

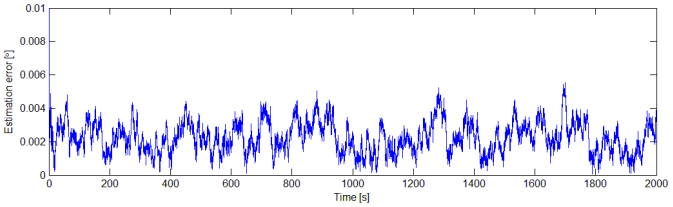

Figure 6 – Estimation with Star Tracker data

The advantages of the variable three vector covariance $Q_{a,k}$ are evidenced when high angular velocities are impressed to the SV. For instance an initial $\|\boldsymbol{\omega}_{init}\| = 10°/s$ results in a biased estimation with a RMS error of $\sigma_{est} = 0.0393°$, whereas using $Q_{a,k}$ produces $\sigma_{est} = 0{,}0289°$.

Drift estimation with the MEKF

We now analyse the drift estimation results of the MEKF with constant parameters. The results of attitude estimation resemble the ones just presented with the major difference being a longer convergence time especially when ad hoc initial attitude guesses are chosen.

In order to test the drift estimation a constant drift of $\boldsymbol{\mu}_{const} = 10^{-5}.[1 \quad -2 \quad -7]^T rad/s$ is introduced in the gyro sensor readings. The initial angular velocity is set to $\boldsymbol{\omega} = 0$. The initial attitude guess is once more at 0,2° from the true attitude. The drift estimate results are presented in Figure 7.

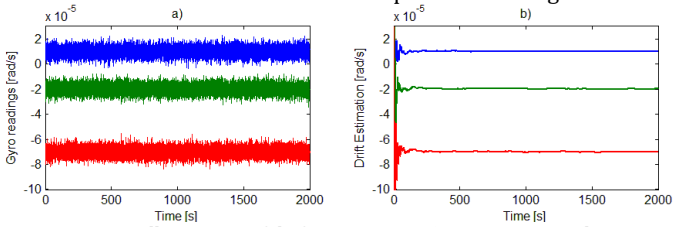

Figure 7 – Illustration of drift estimation: a) Gyroscope readings, b) Drift estimate

A second simulation with the exact same settings but with $\boldsymbol{\omega} = [-0{,}3356 \quad -0{,}0442 \quad -0{,}0854]^T$, $\|\boldsymbol{\omega}\| = 20°/s$, is run. The results are depicted in Figure8.

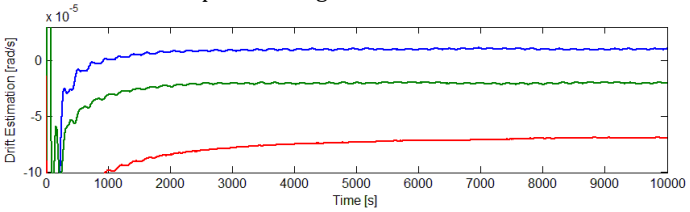

Figure 8 – Drift estimation for nonzero angular velocity

In this situation we observe a longer convergence time, and a small oscillatory behaviour which are due to the extraneous dynamical effect of the rotation of the SV imposed on the filter.

We now compare the difference between the MEKF attitude estimate with and without drift for $\boldsymbol{\omega} = 0$. Figure 9 shows clearly that the error penalty for not estimating the drift is significant.

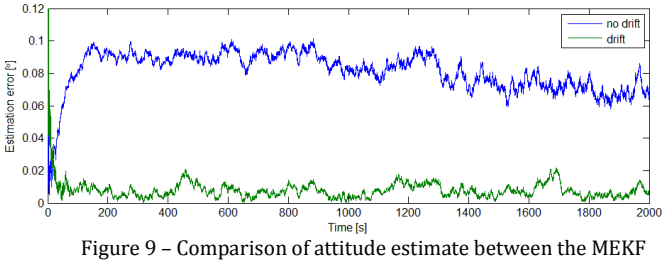

Figure 9 – Comparison of attitude estimate between the MEKF with and with no drift estimate

Single SV Control

In this section the results of attitude control of the single SV system are presented, including steady state operation (equivalent to pointing operation mode), small and large reorientation manoeuvres. Because the MLQR constitutes an augmented version of the simple LQR only results with the MLQR controller will be presented here. In fact for a small manoeuvre ($\Delta\theta < 5°$) the MLQR performs just like the simple LQR.

The wheels speed $\boldsymbol{\omega}_W$ and wheels acceleration $\dot{\boldsymbol{\omega}}_W$ are directly read from free-error sensors.. The Estimator used is the fixed parameter MEKF for attitude estimation only – equivalent to say that the drift has been estimated beforehand. All simulation settings are accordingly as those in the previous chapter.

A small 5° angle manoeuvre is first presented with initial attitude $\bar{q}_{init} = [-0{,}6480 \quad -0{,}5437 \quad -0{,}4473 \quad 0{,}2905]^T$ and null angular ($\boldsymbol{\omega}_{init} = 0$). Figure 10 shows the error evolution during transition to the target. The thrusters perform a faster manoeuvre than the wheels. This behaviour was set up by the tuning of the weighting matrices which gave lesser importance to minimization of thrusters controls.

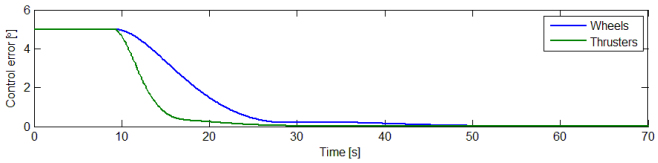

Figure 10 – Small manoeuvre comparison between wheels and thrusters

A large 120° manoeuvre is tested in the same initial conditions as before. The results are depicted in Figure 11.

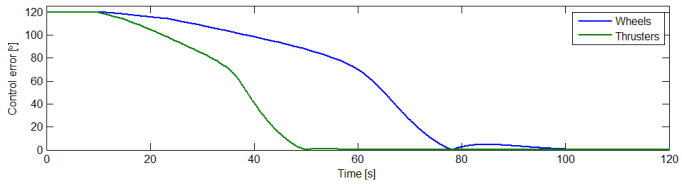

Figure 11 - Large manoeuvre

In most realistic applications the SV might be deployed in orbit with a nonzero angular velocity. Such situation is tested with:
$\boldsymbol{\omega}_{init} = [-0{,}087 \quad 0{,}0038 \quad 0{,}0048]^T\ rad/s \Leftrightarrow \|\boldsymbol{\omega}_{init}\| = 5°/s$, $\bar{q}_{init} = [-0{,}5766 \quad 0{,}3462 \quad -0{,}5867 \quad 0{,}4512]^T$ and an angle displacement of 137,3° for a target quaternion $\bar{q}_{target} = [-0{,}8905 \quad -0{,}0610 \quad 0{,}3915 \quad 0{,}2237]^T$. The results are shown Figure 12.

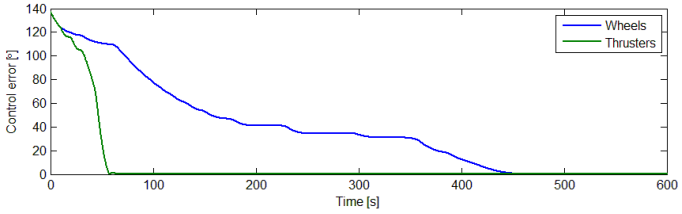

Figure 12 - Control under nonzero initial angular velocity

An evident difference is the manoeuvre time. With wheels actuation the SV wobbles considerable due to the increase in wheels speed that generate gyroscopic momentums.

Figure 13 depicts a period of control under non-ideal actuators following a 10° manoeuvre.

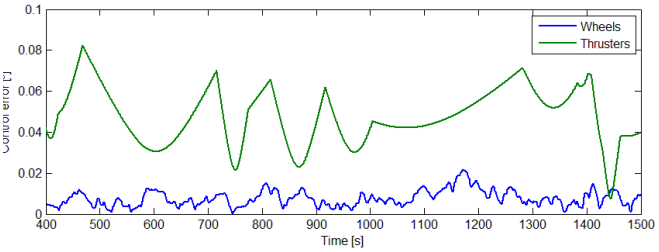

Figure 13 - Control with non-ideal thrusters

The impulsive response of the thrusters is evident whereas reaction wheels render a more controlled mechanism.

In steady-state the pointing RMS errors are as according to Table 4.

Table 4 - Pointing RMS errors with non-ideal thrusters

	Reaction Wheels	Thrusters
Sun and Earth vectors	0,0079°	0,0696°
Star Tracker quaternion	0,0024°	0,0779°

In Figure 14 the result of a fast wheel resetting operation is presented. The initial wheels set speed corresponds to the highest internal angular momentum $\boldsymbol{\omega}_w = [1500 \quad 1500 \quad 1500]^T$ rpm. The control mechanism is able to drive the attitude closer to the target while the wheels speed is damped at a high rate.

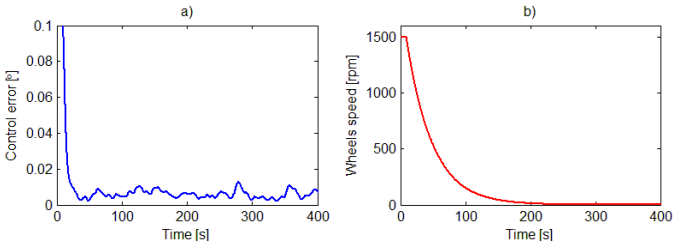

Figure 14 – Reaction wheels resetting manoeuvre

Relative Attitude

Figure 15 demonstrates the feasibility of the relative attitude determination technique using FPD observations for the following formation attitude set:

$$\bar{q}_1 = [0{,}3948 \quad 0{,}5090 \quad -0{,}4679 \quad 0{,}6051]^T$$
$$\bar{q}_2 = [0{,}6923 \quad 0{,}2217 \quad -0{,}6740 \quad 0{,}1320]^T$$
$$\bar{q}_3 = [-0{,}3145 \quad 0{,}0666 \quad 0{,}6496 \quad 0{,}6890]^T$$

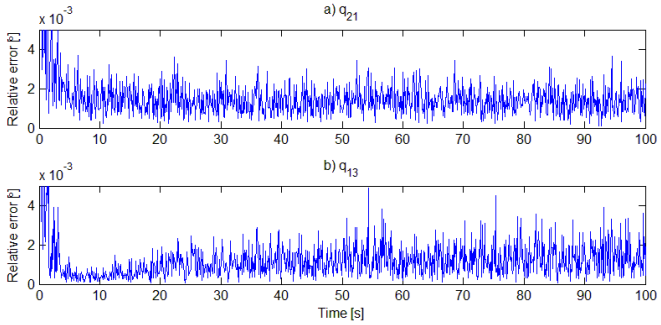

Figure 15 –Relative Attitude Determination error

The RMS errors are $\sigma_{21} = 0{,}0015°$, $\sigma_{13} = 0{,}0015°$, $\sigma_{32} = 0{,}0014°$ for this simulation.

Group Control

Figure 16 shows the results for a simulation where each SV manoeuvres independently to the target $\bar{q}_{target} = [0{,}7298 \quad 0{,}4742 \quad -0{,}4440 \quad 0{,}2128]^T$.

The differences between $\bar{q}_{21}$and $\bar{q}_{13}$ are a consequence of the initial group attitude set and the target attitude, as each SV chooses the shortest path to the target not taking into account the other SVs trajectories.

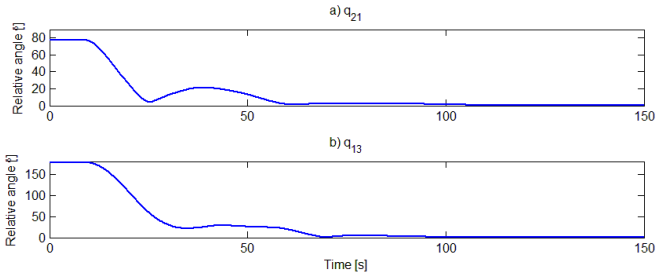

Figure 16 – Independently manoeuvred group

The leader following strategy is shown in Figure 17. Only relative attitude information is feedback into the deputy vehicles SV2 and SV3. The error bumps occur because SV1 establishes a time-varying target for the deputies as it manoeuvres to the final target directly.

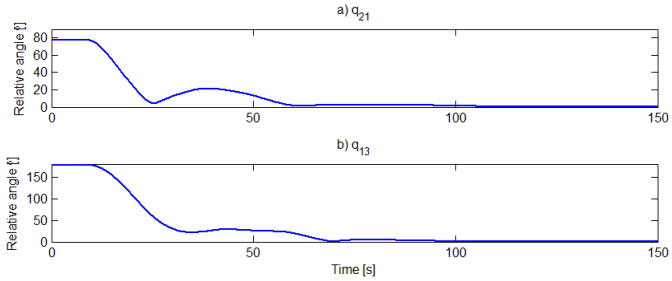

Figure 17 – Leader following strategy

The strategy employing the group coordinator proves to be the fastest manner to reach group alignment as observed in Figure 18. The initial angular separation is large but the group.

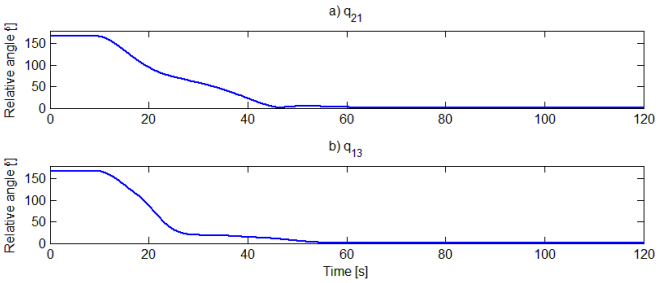

Figure 18 – Group control with converse attitude

IX. Conclusion and Future Work

The tests conducted on the estimation algorithms revealed rapid convergence behaviour and considerable better accuracy compared to the accuracy provided by the deterministic method that solely depends on sensors accuracy.

The MLQR strategy developed is able to drive the SV to the desired attitude although its designed is laborious as its reference setting is logic-based which imposes exhaustive testing to cover all possible transitions. Future work on the controller should address low frequency disturbance rejection with an augmented state system. Additional features may include moving target tracking and angular velocity tracking.

Further work using the developed group control strategy would add features to the coordinator for optimal manoeuvre planning dependent on the initial group configuration, and for varying attitude tracking.

Despite driving the group to the desired attitude, the group control strategy here developed is based on independent attitude tracking from each SV. A cooperative approach would instead describe the formation through a relative attitude model as a set of differential equations on the vehicles states $(\bar{q}_1, \boldsymbol{\omega}_1, \bar{q}_2, \boldsymbol{\omega}_2, \bar{q}_3, \boldsymbol{\omega}_3)$ combinations. This manner the amount of control required for each SV would become correlated with the formation attitude state or a subset of it.

Another interesting feature to explore given a fully equipped group of vehicles is the fact that relative attitude information provides redundant inertial attitude estimates which may be used to mitigate sensor misalignment errors.

[1] Wertz, James R. *Spacecraft Attitude Determination and Control*, Dordrecht, Kluwer Academic Publishers, 1978

[2] Yonatan Winetraub, San Bitan & Uval dd & Anna B. Heller. *Attitude Determination – Advanced Sun Sensors for Pico-satellites*, Handasaim School, Tel-Aviv University, Israel

[3] Rycroft, Michael J. Stengel, Robert F. *Spacecraft Dynamics and Control*, Cambridge University Press 1997

[4] William E. Wiesel, *Spaceflight Dynamics*, Irwin McGraw-Hill, 2nd Edition

[5] Malcolm D. Shuster, *Deterministic Three-Axis Attitude Determination*, The Journal of the Astronautical Sciences, Vol. 52, No. 3, July-September 2004, pp. 405-419

[6] Maria Isabel Ribeiro, *Kalman and Extended Kalman Filters: Concept, Derivation and Properties*, Institute for Systems and Robotics, Instituto Superior Técnico, February 2004

[7] Balbach, Oliver & Eissfeller, Bernd & Gunter W. Hein. *Tracking GPS above GPS Satellite Altitude: First Results of the GPS experiment on the HEO Mission Equator-S*

[8] F. Landis, Markley, *Multiplicative vs. Additive Filtering for Spacecraft Attitude Determination,* NASA's Goddard Space Flight Center

[9] F. Landis, Markley, *Attitude Estimation or Quaternion Estimation?*, NASA's Goddard Space Flight Center

[10] Richard M. Murray, Zexiang Li, S. Shankar Sastry, *A Mathematical Introduction to Robotic Manupulation*, chapter 2. CRC Press, 1994

[11] Grace Wahba, *A Least Squares Estimate of Satellite Attitude*. SIAM Review, Vol. 8, No. 3, (Jul., 1966), 384-286

[12] F. Landis Markley, "*Fast Quaternion Attitude Estimation from Two Vector Measurements"* Guidance, Navigation and Control Systems Engineering Branch, code 571. NASA's Goddard Space Flight Center, Greenbelt, MD20771

[13] J. Miranda Lemos, "*Introdução ao Controlo Óptimo*", Class notes. IST 2012

[14] HE BAi, Murat Arcak, John Wen," *Cooperative Control Design: A Systematic, Passivity-Based Approach*". Springer

[15] Michael S. Andrle, Baro Hyun, John L. Crassidis, Richard Linares, "*Deterministic Relative Attitude Determination of Formation Flying Spacecraft*". University of Buffalo, State University of New York, Amherst, NY, 14260-4400

[16] Rand W. Beard, Jonathan Lawton, Fred Hadaegh, "*A Coordinated Architecture for Spacecraft Formation Control*". IEEE Transactions on Control systems Technology, Vol. 9, No. 6, 2001

[17] Robert Strengel, "Spacecraft Sensors and Actuators", Space System Design, MAE 342, Princeton University

[18] Malcolm D. Shuster, "Deterministic Three-Axis Attitude Determination", The Journal of the Astronautical Sciences, Vol. 52, pp. 405–419